Generating Single-Spike Hard X-Ray Pulses with Nonlinear Bunch Compression in Free-Electron Lasers

S. Huang,[1] Y. Ding,[2,*] Y. Feng,[2] E. Hemsing,[2] Z. Huang,[2] J. Krzywinski,[2] A. A. Lutman,[2] A. Marinelli,[2] T. J. Maxwell,[2] and D. Zhu[2]

[1]*Institute of Heavy Ion Physics, School of Physics, Peking University, Beijing 100871, China*

[2]*SLAC National Accelerator Laboratory, Menlo Park, California 94025, USA*

(Received 12 May 2017; published 10 October 2017)

A simple method for generating single-spike hard x-ray pulses in free-electron lasers (FELs) has been developed at the Linac Coherent Light Source (LCLS). This is realized by nonlinear bunch compression using 20-pC bunch charge, demonstrated in the hard x-ray regime at 5.6 and 9 keV, respectively. Measurements show about half of the FEL shots containing a single-spike spectrum. At 5.6-keV photon energy, the single-spike shots have a mean pulse energy of about 10 μJ with 70% intensity fluctuation and the pulse full width at half maximum is evaluated to be at 200-as level.

DOI: 10.1103/PhysRevLett.119.154801

During the past few decades, great efforts have been made in generating attosecond radiation [1–3]. These pulses offer an opportunity for studying electronic dynamics on the atomic or molecular scale and are expected to inspire new breakthroughs in ultrafast sciences [4,5]. Presently attosecond radiation pulses are mostly generated by high-order harmonic generation (HHG) technique with photon energy typically up to a few hundred eV [6]. Extending the spectral range to the keV level has been recently demonstrated [7], but the obtained harmonic yields are very low.

Free-electron lasers (FELs) [8–10] provide an alternative way for generating intense ultrashort radiation pulses at the keV energy regime, and a few facilities have been successfully operated in recent years [11–14]. Nowadays most of the x-ray FELs are based on a self-amplified spontaneous emission (SASE) mechanism. In such FELs, the radiation copropagates with the electron bunch along the FEL undulator and the initial low-power radiation source, originating from the spontaneous emission of the electron bunch, gets amplified through interaction with the electrons until the process saturates. The total radiation pulse duration is therefore determined by the lasing part of the electron bunch, which is typically tens of femtoseconds (fs) long containing many temporal spikes. The width of one single spike in the hard x-ray SASE radiation is, determined by coherence length [10], typically about 200–300 as.

To further shorten the total pulse duration down to the attosecond regime, various ideas have been proposed with the x-ray FELs [15–34]. A common way is based on time slicing of the electron bunch, in which the lasing part of the electron bunch is selectively controlled by an extremely short optical laser pulse, by a slotted foil, or by a bunch tilt with subsequent orbit control [15–29]. The slicing scheme uses an electron beam with a regular bunch charge, but requires implementing additional hardware in the existing facility. At the Linac Coherent Light Source (LCLS), a slotted foil [35] has been installed for short pulse operation [36]. Recently, a dechirper device [37] has also become available at the LCLS which has been used for lasing control with a bunch tilt [38]. They are both established short-pulse operating modes in the femtosecond regime. As far as we know, the only demonstrated attosecond x-ray FEL is the recent measurement using an upgraded slotted foil at the LCLS [34]. Another way is reducing the bunch charge dramatically (e.g., 1 pC) together with strong compression [31–33]. This extreme low-charge mode (~2 orders lower than the designed FEL machines) imposes extra requirements on the electron beam diagnostics and accelerator stability.

In this Letter, we report experimental demonstration of generating single-spike sub-fs hard x-ray FEL pulses at the LCLS with a recently proposed nonlinear bunch compression scheme [39]. This is realized by optimizing the voltage and phase of an existing high-harmonic radio-frequency (rf) structure, through which a nonlinearly curved electron distribution in the longitudinal (time-energy) phase space is formed after bunch compression. The electron current profile is then comprised of a high-current leading peak (a horn) and a long low-current tail. As a result, the FEL process can be restricted within the leading peak enabling much shorter x-ray pulses compared to the electron bunch. This method can be applied directly to any existing x-ray FEL facility since no additional hardware is required.

The LCLS, as sketched in Fig. 1, comprises a 135-MeV injector (not shown in the figure), a 1-km-long linac with two four-dipole chicane bunch compressors (BC1 and BC2) at 220 MeV and 5 GeV, respectively, a 132-m-long undulator line, and transport beam lines [12]. The linac includes three sections of *S*-band rf traveling-wave structures at 2.856 GHz (L1S, L2, and L3) and one fourth-harmonic *X*-band rf section (L1X). The electron bunch is longitudinally compressed by BC1 and BC2. To do this, we accelerate the electrons at an off-crest rf phase so that the

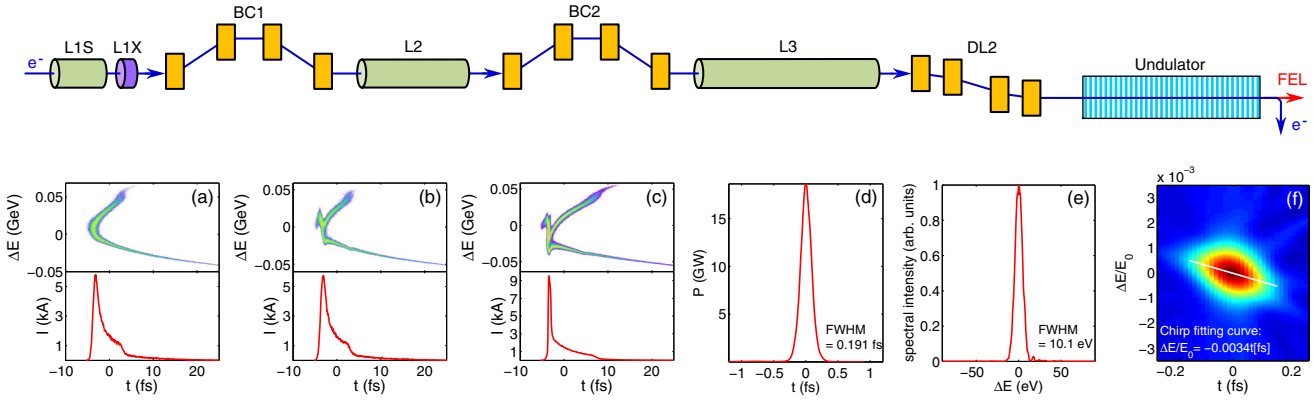

FIG. 1. A sketch of nonlinear bunch compression at the LCLS. At the top is a layout of the LCLS, with main linac *S*-band sections (L1S, L2, L3), one *X*-band linac section (L1X), two bunch compressor chicanes (BC1 and BC2), a dog-leg beam line (DL2), and an undulator. The bottom plots show simulated longitudinal phase space and current profile after BC2 (a), L3 exit (b), and undulator entrance (c), and FEL simulation results, including power profile (d), spectrum (e) and Wigner transformation of the FEL field (f). The FEL photon energy in this simulation is 5.6 keV. Bunch head is to the left.

electron bunch has a time-energy chirp. During the passage through the chicane, the high-energy tail travels a shorter path to catch up with the low-energy head so that the bunch is compressed in time. In regular FEL operation, the time-energy chirp before the compressor is expected to be linear in order to generate a uniform final current profile. This is realized by the fourth-harmonic rf structure L1X through decelerating the electron beam, which cancels the *S*-band rf-curvature induced nonlinear correlation [40]. Accordingly, we call the harmonic structure a phase space "linearizer" in regular FEL operation.

In the nonlinear compression scheme, as studied here, we intentionally reduce the amplitude of the fourth-harmonic rf structure L1X so that the electron bunch has a nonlinear time-energy chirp. During BC2 compression, we set the middle part of the bunch to get fully compressed while the head and tail are compressed differently. As a result, a "banana"-shaped electron distribution in the longitudinal phase space is formed after BC2, and the resultant current profile has a high-current leading peak together with a low-current tail [see Fig. 1(a)]. This distribution is similar to that achieved in the early operation stage of FLASH before adding a linearizer [41], but here we can control the curvature of the nonlinear longitudinal phase space to get a stable, high-current spike by optimizing the L1X parameters.

The longitudinal space charge (LSC) force downstream BC2 becomes an important factor in the system, which pushes the electrons near the horn head (tail) to higher (lower) energy. The strength of the LSC fields depends on the derivative of the electron beam current. As a result, the strong LSC force in the horn region forms a time-energy chirp with higher energy on the front, as seen in Figs. 1(b) and 1(c). Fortunately, this time-energy chirp can be leveraged by reversely tapering the undulator field strength, i.e., increasing the field strength along the undulator [19,42]. As the radiation slips forward with respect to the bunch, it interacts with higher-energy electrons at stronger undulator fields, and the FEL resonance condition is preserved. Since the chirp in the core is distinguished from other parts, the taper we choose according to the core part not only maintains lasing on the current horn, but also suppresses lasing elsewhere, which further shortens the x-ray pulse duration [39]. As shown in Figs. 1(d) and 1(e), simulations predict the production of single-spike x-ray pulses with a full width at half maximum (FWHM) duration around 200 as and a 10 eV FWHM bandwidth.

In the nonlinear compression experiment at the LCLS, we chose the bunch charge to be 20 pC, which is the lowest charge established for short pulse (< 10 fs) operation [43] at the LCLS determined by the diagnostics sensitivity. Starting from a regular operating mode with linear compression (L1X voltage set at 19–20 MV, phase at $-160°$), we only need some minor adjustments of the linac rf parameters to realize nonlinear compression. The rf amplitude of L1X was reduced first, together with L1S adjustment for maintaining the energy and current after BC1 at the same values as in the linear compression setup. Then we scanned the L2 phase (the L2 amplitude is adjusted accordingly to keep a constant energy gain in L2) to find the minimum bunch length using the BC2 bunch length monitor (BLM) [44]. According to the measured electron profile and FEL spectra, the L1X amplitude and phase are further optimized. A list of the main LCLS parameters for nonlinear compression configuration is shown in Table I.

Longitudinal diagnosis of the electron beam is a critical part for carrying out this experiment. We have three longitudinal diagnostic systems available at the LCLS: a relative BLM after BC2 [45], an *X*-band rf transverse deflector (XTCAV) downstream of the undulator [46], and a middle-infrared (MIR) prism spectrometer before the undulator [47]. The BLM is based on coherent edge radiation from the last bend magnet of the compressor

TABLE I. The LCLS parameters for nonlinear bunch compression experiment.

Parameter	Value	Unit
Bunch charge	20	pC
Injector bunch length (FWHM)	850	μm
DL1 energy	135	MeV
DL1 R56	6.3	mm
L1S rf phase	−27	deg
L1X rf phase	−170– − 180	deg
L1X rf amplitude	12–15	MV
BC1 energy	220	MeV
BC1 R56	−45.5	mm
L2 rf phase	−35.4– − 34.8	deg
BC2 energy	5	GeV
BC2 R56	−24.7	mm
L3 rf phase	0	deg
DL2 energy	11–14	GeV
DL2 R56	0.133	mm

chicane. It is a noninterceptive, single-shot measurement calibrated by a transverse deflector at 150–250 pC [44]. At this 20 pC charge, no calibration has been made but it still provides a fast way to roughly determine the compression mode. (The signal peaks at full compression.) Starting from the undercompression side, increasing the chirp makes a maximum (full) compression on the bunch head (other parts are still undercompressed), resulting in a leading current spike. After that, a small increase of the chirp shifts the full compression section towards the bunch center, while the head is overcompressed and the tail is still undercompressed. This is the desired operating point with a banana shape. A further increase in the chirp makes the whole bunch overcompressed, where the bunch head and tail are switched. Operating in the longer pulse range, as in the undercompression or overcompression, it is possible to measure the time-energy phase space distribution with the XTCAV. However, measuring the phase-space of the banana-shaped beam is beyond the XTCAV resolution (the resolution with upgraded SLED mode [48] is about 2 fs rms [49] at the high energy range above 10 GeV). For this extremely short bunch, the MIR prism spectrometer provides a better resolution to guide the setup.

The MIR prism spectrometer diagnostic is based on measuring the power spectrum of the light produced by an electron bunch undergoing a coherent transition radiation process with a thin foil. While we scan the L2 phase, the bunch length after the BC2 compressor is varied and each single shot spectrum is recorded. We show the spectral measurements with the MIR prism spectrometer in Fig. 2 with electron beam energy at 14 GeV. The 2D plot shows spectral intensity distribution as a function of the L2 phase and the radiation spatial frequency $\kappa \equiv 1/\lambda$ (λ is the transition radiation wavelength), where the maximum bandwidth ($\Delta\kappa$) corresponds to minimum bunch length

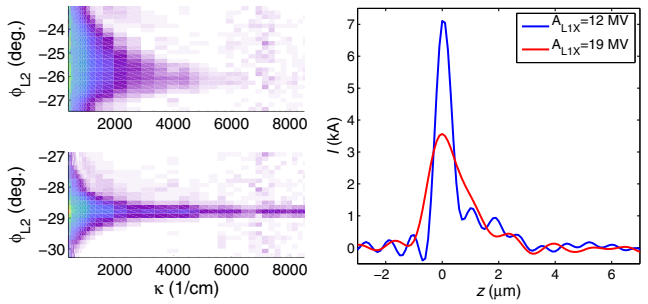

FIG. 2. (left) Spectral measurement using the MIR prism spectrometer versus L2 phase at linear (top, L1X at 19 MV) and nonlinear (bottom, L1X at 12 MV) compression. (right) Two reconstructed current profile examples at minimum achieved pulse duration for linear and nonlinear compression. Electron beam energy was 14 GeV, bunch charge was 20 pC.

(maximum compression). Note the BLM signal is also recorded simultaneously during the MIR prism measurement, and we see a good correlation between the bandwidth from the MIR spectrometer and the BLM signal intensity. From Fig. 2, one can see the measured maximum bandwidth at the nonlinear compression mode (L1X at 12 MV) is clearly larger compared to the one at linear compression (L1X at 19 MV). The electron current profile can be retrieved from the measured spectral profile by the Kramers-Kronig phase reconstruction method (see details in Ref. [47] and references therein). We show two examples of the reconstructed current profile at the maximum compression, with L1X at 12 MV and 19 MV, respectively. As shown in Fig. 2, at nonlinear compression, the peak current is increased by about a factor 2 with bunch duration about 1 μm (3 fs) FWHM. Note that with these extremely short pulses, the measurement is still limited by instrument resolution with high-frequency content clearly extending just beyond the range of the spectrometer, and so this is still only an upper limit of the pulse duration.

The nonlinearly compressed electron bunch was then transported to the LCLS undulator for producing x rays. As discussed earlier, the LSC induces a distinguished chirp at the core part of the bunch. Inside the undulator, the LSC force is even stronger due to wiggling motion [50], further enhancing the time-energy chirp within the electron bunch. During the experiment, we applied a linear reverse taper to counteract this chirp effect.

Temporal characterization of these short x-ray pulses is very challenging. Instead, spectral domain diagnosis provides an alternative way [42,51]. At the LCLS, a transmissive hard x-ray single-shot spectrometer has been developed [52,53]. Based on the Bragg reflection of a parallel incoming x-ray by a cylindrically bent silicon crystal, the spectrometer has a wide spectral range in the hard x-ray regime and a resolution at sub-eV level, which is sufficient to resolve individual SASE spectral spikes in the experiment.

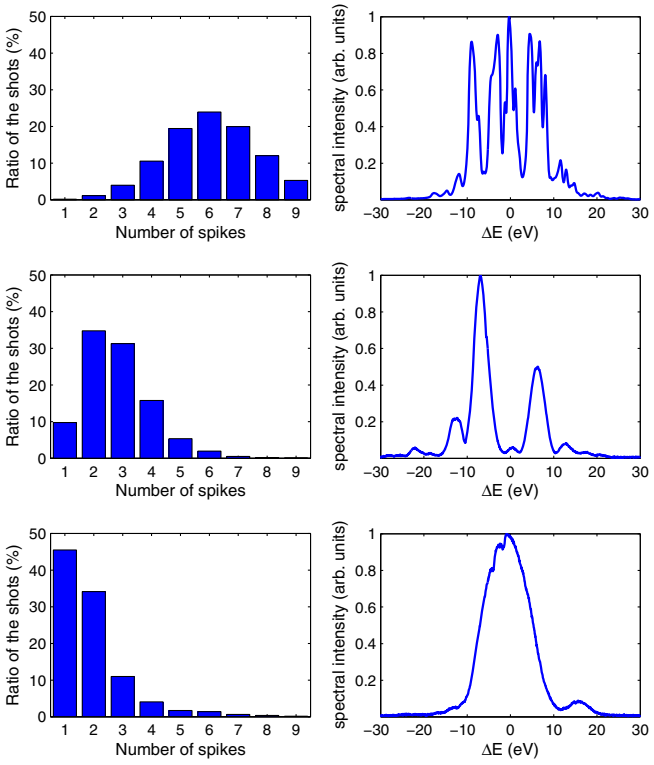

FIG. 3. Histogram of the number of spikes (left) and measured spectral example (right) at 9 keV versus the L1X voltage: (top) 19 MV; (middle) 15 MV and (bottom) 12 MV. Each setting used 2000 shots. Electron beam energy was 14 GeV, bunch charge was 20 pC.

Figure 3 shows the FEL spectrum evolution while switching the LCLS from the regular linear compression mode to the nonlinear compression mode at the photon energy of 9 keV. The electron beam energy is 14 GeV. Each histogram in Fig. 3 (left column) was computed based on 2000 consecutive shots. We see that in the regular linear compression mode (without reverse tapering), most of the shots have 5–7 spikes. By reducing the L1X voltage to 15 MV (with adding a reverse taper of 5.5×10^{-5} m^{-1} from undulator U17 to U32), the number of spikes in each shot is reduced, with more than half of the shots presenting 2–3 spikes. Lowering L1X to 12 MV, we achieved most of the shots with single or double spikes as shown in the figure. The average pulse energy of the single-spike shots is about 7 ± 4 μJ. If we further reduce L1X to 10 MV, the histogram of the spike number is similar to the case at 12 MV, but the average pulse energy is reduced to 4 ± 3 μJ. This means that further reducing the L1X amplitude would preserve a current spike but with lower current value, which degrades the FEL performance. For this 9-keV photon beam, we concluded that L1X at 12 MV is an optimal condition. We kept a constant reverse tapering for all the reduced L1X amplitudes of 10–15 MV. The FEL performance was not sensitive to the tapering variation within a range of $\pm 10\%$, probably because a rather long undulator was used in the experiments. The right column of Fig. 3 shows one typical spectrum recorded at each setting. As we can see, the number of spikes is reduced and the spike width is increased while lowering the L1X voltage. Based on the statistical theory, the pulses should have a similar number of spikes in time domain.

More measurements were performed at the x-ray photon energy of 5.6 keV, with electron beam energy at 11.5 GeV. After optimization, we chose the L1X at 13 MV which produces the highest ratio of single-spike pulses. A reverse tapering of 5.0×10^{-5} m^{-1} was applied from undulator U7 to U32. In Fig. 4, we plot the histogram of the number of spikes calculated on a data set with 8400 consecutively recorded spectra. About 50% of the shots have a single spike. After sorting the shots according to the number of spikes, the average energy for the single-spike shots was about 10 μJ with 70% fluctuation. We also show ten continuous single-spike spectral examples choosing from the sorted single-spike group. The FWHM bandwidth of these measured single-spike spectra, obtained through Gaussian fitting, was 11.3 ± 4.2 eV. Such a bandwidth yields a duration of 162 ± 60 as FWHM assuming that the pulses have Fourier-transform-limited Gaussian distribution. However, as the FEL was generated by time-energy chirped electrons herein, the radiation presents a frequency chirp leading to an underestimate of the pulse length.

To estimate the FEL pulse duration, we used a simple model assuming a linearly chirped Gaussian pulse [54]. With this model, the FWHM pulse duration, τ_p, can be calculated using

$$\tau_p = \frac{2\sqrt{2}\ln 2/\pi}{\sqrt{\Delta f_p^2 + \sqrt{\Delta f_p^4 - (4\ln 2 \alpha f_0/\pi)^2}}}, \qquad (1)$$

where Δf_p is the spectral FWHM in Hz, f_0 is the central frequency in Hz, α is the frequency chirp parameter defined as the relative change of instantaneous frequency over time

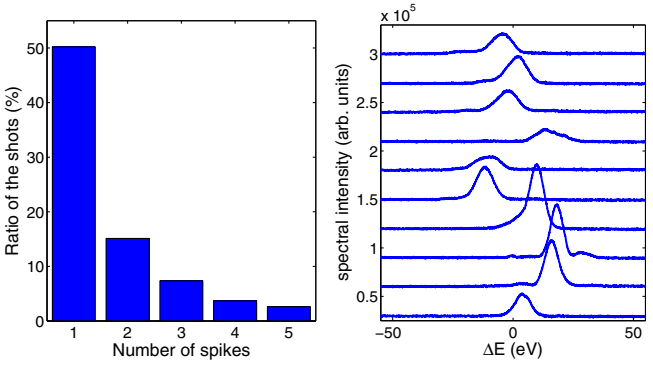

FIG. 4. (left) Histogram of the number of spectral spikes based on 8400 shots. (right) Ten recorded shots of the sorted single-spike x-ray spectra (at 5.6 keV). Electron beam energy was 11.5 GeV, bunch charge was 20 pC. L1X amplitude was 13 MV.

Δt, i.e., $\alpha = \Delta f/f_0/\Delta t$. As discussed in the Supplemental Material [55], typically there are two solutions of the pulse duration for a given pulse spectral bandwidth and chirp, and the solution we are using from Eq. (1) is benchmarked with simulation results. An accurate measurement of the frequency chirp is unavailable in the experiment. Note that Eq. (1) has an upper limit of $\tau_{p,\max} = 2\sqrt{2}\ln 2/(\pi\Delta f_p)$ when $|\alpha| = \pi\Delta f_p^2/(4\ln 2 f_0)$, a maximum achievable frequency chirp in absolute value at a given spectral width and central frequency. So we can estimate the upper limit of FWHM pulse duration to be 228 ± 85 as for the single-spike shots at 5.6 keV using measured bandwidth 11.3 ± 4.2 eV. A similar estimate for the 9 keV single-spike data (FWHM bandwidth is 14.4 ± 4.7 eV with L1X at 12 MV) gives an upper limit of the FWHM pulse duration of 179 ± 58 as.

In conclusion, we have demonstrated a simple way for generating single-spike hard x-ray FEL pulses at the LCLS. We measured single-spike pulses with estimated FWHM pulse duration at the 200-as level at 5.6 and 9 keV. We expect to have a similar performance in a range of 4–10 keV, and in principle this scheme should also work in the soft x-ray regime. Because of a larger slippage length at soft x-ray FELs, a single spike width is expected to be about 1–2 fs.

This work is supported by the U.S. Department of Energy Contract No. DE-AC02-76SF00515 and the National Key Research and Development Program of China (Grant No. 2016YFA0401904).

*ding@slac.stanford.edu

[1] G. Sansone, L. Poletto, and M. Nisoli, Nat. Photonics **5**, 655 (2011).
[2] M. Chini, K. Zhao, and Z. Chang, Nat. Photonics **8**, 178 (2014).
[3] Z. Chang and P. Corkum, J. Opt. Soc. Am. B **27**, B9 (2010).
[4] P. H. Bucksbaum, Science **317**, 766 (2007).
[5] F. Krausz and M. Ivanov, Rev. Mod. Phys. **81**, 163 (2009).
[6] K. Midorikawa, Jpn. J. Appl. Phys. **50**, 090001 (2011).
[7] T. Popmintchev, M.-C. Chen, D. Popmintchev, P. Arpin, S. Brown, S. Ališauskas, G. Andriukaitis, T. Balčiunas, O. D. Mücke, A. Pugzlys, A. Baltuška, B. Shim, S. E. Schrauth, A. Gaeta, C. Hernández-García, L. Plaja, A. Becker, A. Jaron-Becker, M. M. Murnane, and H. C. Kapteyn, Science **336**, 1287 (2012).
[8] Z. Huang and K.-J. Kim, Phys. Rev. ST Accel. Beams **10**, 034801 (2007).
[9] B. W. J. McNeil and N. R. Thompson, Nat. Photonics **4**, 814 (2010).
[10] K.-J. Kim, Z. Huang, and R. Lindberg, *Synchrotron Radiation and Free-Electron Lasers* (Cambridge University Press, Cambridge, England, 2017).
[11] W. Ackermann *et al.*, Nat. Photonics **1**, 336 (2007).
[12] P. Emma *et al.*, Nat. Photonics **4**, 641 (2010).
[13] T. Ishikawa *et al.*, Nat. Photonics **6**, 540 (2012).
[14] E. Allaria *et al.*, Nat. Photonics **7**, 913 (2013).
[15] E. Hemsing, G. Stupakov, D. Xiang, and A. A. Zholents, Rev. Mod. Phys. **86**, 897 (2014).
[16] E. L. Saldin, E. A. Schneidmiller, and M. V. Yurkov, Opt. Commun. **237**, 153 (2004).
[17] E. L. Saldin, E. A. Schneidmiller, and M. V. Yurkov, Opt. Commun. **239**, 161 (2004).
[18] A. A. Zholents, Phys. Rev. ST Accel. Beams **8**, 040701 (2005).
[19] E. L. Saldin, E. A. Schneidmiller, and M. V. Yurkov, Phys. Rev. ST Accel. Beams **9**, 050702 (2006).
[20] A. A. Zholents and M. S. Zolotorev, New J. Phys. **10**, 025005 (2008).
[21] Y. Ding, Z. Huang, D. Ratner, P. Bucksbaum, and H. Merdji, Phys. Rev. ST Accel. Beams **12**, 060703 (2009).
[22] J. Qiang and J. Wu, Appl. Phys. Lett. **99**, 081101 (2011).
[23] J. Qiang and J. Wu, J. Mod. Opt. **58**, 1452 (2011).
[24] P. Emma, Z. Huang, and M. Borland, *Proceedings of FEL Conference (FEL2004)*, (Comitato Conferenze Elettra, Trieste, Italy 2005), p. 333.
[25] N. R. Thompson and B. W. J. McNeil, Phys. Rev. Lett. **100**, 203901 (2008).
[26] D. J. Dunning, B. W. J. McNeil, and N. R. Thompson, Phys. Rev. Lett. **110**, 104801 (2013).
[27] T. Tanaka, Phys. Rev. Lett. **110**, 084801 (2013).
[28] E. Prat and S. Reiche, Phys. Rev. Lett. **114**, 244801 (2015).
[29] E. Prat, F. Lohl, and S. Reiche, Phys. Rev. ST Accel. Beams **18**, 100701 (2015).
[30] E. L. Saldin, E. A. Schneidmiller, and M. V. Yurkov, Opt. Commun. **212**, 377 (2002).
[31] J. B. Rosenzweig, D. Alesini, G. Andonian, M. Boscolo, M. Dunning, L. Faillace, M. Ferrario, A. Fukusawa, L. Giannessi, E. Hemsing, G. Marcus, A. Marinelli, P. Musumeci, B. O'Shea, L. Palumbo, C. Pellegrini, V. Petrillo, S. Reiche, C. Ronsivalle, B. Spataro, and C. Vaccarezza, Nucl. Instrum. Methods Phys. Res., Sect. A **593**, 39 (2008).
[32] S. Reiche, P. Musumeci, C. Pellegrini, and J. B. Rosenzweig, Nucl. Instrum. Methods Phys. Res., Sect. A **593**, 45 (2008).
[33] V. Wacker, Y. Ding, J. Frisch, Z. Huang, C. Pellegrini, and F. Zhou, *Proceedings of FEL2012*, (JACoW, Nara, Japan 2012), p. 606.
[34] A. Marinelli, Appl. Phys. Lett. (to be published).
[35] P. Emma, K. Bane, M. Cornacchia, Z. Huang, H. Schlarb, G. Stupakov, and D. Walz, Phys. Rev. Lett. **92**, 074801 (2004).
[36] Y. Ding, C. Behrens, R. Coffee, F. J. Decker, P. Emma, C. Field, W. Helml, Z. Huang, P. Krejcik, J. Krzywinski, H. Loos, A. Lutman, A. Marinelli, T. J. Maxwell, and J. Turner, Appl. Phys. Lett. **107**, 191104 (2015).
[37] Z. Zhang, K. Bane, Y. Ding, Z. Huang, R. Iverson, T. Maxwell, G. Stupakov, and L. Wang, Phys. Rev. ST Accel. Beams **18**, 010702 (2015).
[38] A. A. Lutman *et al.*, Nat. Photonics **10**, 745 (2016).
[39] S. Huang, Y. Ding, Z. Huang, and J. Qiang, Phys. Rev. ST Accel. Beams **17**, 120703 (2014).
[40] P. Emma, LCLS Technical Note Report No. SLAC-TN-05-004 (2001).
[41] M. Dohlus, K. Floettmann, O. S. Kozlov, T. Limberg, P. Piot, E. L. Saldin, E. A. Schneidmiller, and M. V. Yurkov, Nucl. Instrum. Methods Phys. Res., Sect. A **530**, 217 (2004).

[42] L. Giannessi *et al.*, Phys. Rev. Lett. **106**, 144801 (2011).
[43] Y. Ding, A. Brachmann, F.-J. Decker, D. Dowell, P. Emma, J. Frisch, S. Gilevich, G. Hays, P. Hering, Z. Huang, R. Iverson, H. Loos, A. Miahnahri, H.-D. Nuhn, D. Ratner, J. Turner, J. Welch, W. White, and J. Wu, Phys. Rev. Lett. **102**, 254801 (2009).
[44] H. Loos, Advances in X-ray Free-Electron Lasers II: Instrumentation, *Proc. SPIE 8788* (SPIE, Prague, Czech, 2013), p. 87780J.
[45] H. Loos, T. Borden, P. Emma, J. C. Frisch, and J. Wu, *Proceedings of PAC07* (JACoW, Albuquerque, New Mexico, USA, 2007), p. 4189.
[46] C. Behrens, F. J. Decker, Y. Ding, V. A. Dolgashev, J. Frisch, Z. Huang, P. Krejcik, H. Loos, A. Lutman, T. J. Maxwell, J. Turner, J. Wang, M. H. Wang, J. Welch, and J. Wu, Nat. Commun. **5**, 3762 (2014).
[47] T. J. Maxwell, C. Behrens, Y. Ding, A. S. Fisher, J. Frisch, Z. Huang, and H. Loos, Phys. Rev. Lett. **111**, 184801 (2013).
[48] J. Wang, G. Bowden, S. Condamoor, Y. Ding, V. Dolgashev, J. Eichner, M. Franzi, A. Haase, P. Krejcik, J. Lewandowski, S. Tantawi, L. Xiao, and C. Xu, *Proceedings of IPAC2016*, (JACoW, Busan, Korea 2016), p. 39.
[49] P. Krejcik, G. Bowden, S. Condamoor, Y. Ding, V. Dolgashev, J. Eichner, M. Franzi, A. Haase, J. Lewandowski, T. Maxwell, S. Tantawi, J. Wang, L. Xiao, and C. Xu, *Proceedings of IBIC2016*, (JACoW, Barcelona, Spain 2016), p. 833.
[50] G. Geloni, Nucl. Instrum. Methods Phys. Res., Sect. A **583**, 228 (2007).
[51] Y. Inubushi, K. Tono, T. Togashi, T. Sato, T. Hatsui, T. Kameshima, K. Togawa, T. Hara, T. Tanaka, H. Tanaka, T. Ishikawa, and M. Yabashi, Phys. Rev. Lett. **109**, 144801 (2012).
[52] D. Zhu, M. Cammarata, J. M. Feldkamp, D. M. Fritz, J. B. Hastings, S. Lee, H. T. Lemke, A. Robert, J. L. Turner, and Y. Feng, Appl. Phys. Lett. **101**, 034103 (2012).
[53] D. Rich, D. Zhu, J. Turner, D. Zhang, B. Hill, and Y. Feng, J. Synchrotron Radiat. **23**, 3 (2016).
[54] A. E. Siegman, *Lasers* (University Science Books, Sausalito, California, 1986), p. 332.
[55] See Supplemental Material at http://link.aps.org/supplemental/10.1103/PhysRevLett.119.154801 for a brief discussion about calculating the temporal duration from a linearly chirped Gaussian pulse.